

## At substorm onset, 40% of AL comes from underground

E. I. Tanskanen, A. Viljanen, T. I. Pulkkinen, R. Pirjola, L. Häkkinen,  
A. Pulkkinen and O. Amm

Geophysical Research Division, Finnish Meteorological Institute, Helsinki, Finland

**Abstract.** Magnetic variations observed at the Earth's surface are caused by external and internal sources. External variations arise from currents in the ionosphere and magnetosphere, and internal variations arise from currents induced in the solid Earth. In this paper we examine how large the internal contribution is to magnetic variations measured at the Earth's surface. We use IMAGE magnetometer measurements to analyze 77 substorms during 1997. For each event we evaluate the internal and external parts of a locally derived auroral electrojet index (*IL* index). The magnetic field separation is performed using the Siebert-Kertz equations. A superposed epoch analysis of all events clearly shows that the internal contribution peaks strongly at substorm onset, when the internal contribution is  $\sim 40\%$  of the total field. After the substorm peak intensity, the internal contribution decreases almost linearly to the quiet time value of 10–20%. The induction effects are largest during the times of rapid changes and at stations located over the Arctic Ocean.

### 1. Introduction

The auroral electrojet indices, *AU* and *AL* [Davis and Sugiura, 1966], are defined as maximal positive and negative variations in the *X* components of 12 auroral-latitude magnetometer stations. Determined this way, the indices give a measure of the large scale eastward (*AU*) and westward (*AL*) electrojet intensities [e.g., Vassiliadis et al., 1995]. However, the global indices become available only several years after the measurements, and they do not give an accurate representation of the current intensity under situations where the main part of the current is far away from the standard stations [Kauristie et al., 1996]. Consequently, local (latitudinal) chains are often used to create local electrojet indices such as the *CU/CL* indices from the CANOPUS chain in Canada [Rostoker et al., 1995] or the *IU/IL* indices from the IMAGE magnetometer array in Fennoscandia and Svalbard [Kallio et al., 2000]. These local indices measure only the currents in the local time sector covered by the chain but have the advantage of covering an extended range of latitudes and hence having a better chance of recording the maximum disturbance underneath the center of the electrojet [Kauristie et al., 1996].

The auroral electrojet indices have been widely used in various studies concerning the solar wind-magnetosphere-ionosphere coupling [e.g., Vassiliadis et al., 1995]. In this coupled system, solar wind energy that enters

the magnetosphere is partially dissipated in the inner magnetosphere ring current region, partially deposited into the ionosphere, and partially ejected from the magnetosphere with plasma flows along the tail [Lu et al., 1998; Ieda et al., 1998]. Establishing the routes of energy dissipation and their relative importance is a key element in resolving the open issues related to, for example, magnetospheric substorm processes [Baker et al., 1996]. Furthermore, the auroral electrojets are also directly driven by the solar wind impinging on the dayside magnetosphere: Several studies utilizing linear and nonlinear filtering techniques have demonstrated a high degree of predictability of the *AL* index using present and past values of the solar wind, interplanetary magnetic field, and of the *AL* index itself [Bargatze et al., 1985; Baker et al., 1990; Vassiliadis et al., 1995]. These methods are being further developed to provide reliable estimators of near-future geomagnetic activity conditions for space weather purposes.

It is clear from the above that the auroral electrojet indices and their local variants play a key role in modern space physics as well as in the development of space weather nowcasts and forecasts. Therefore it is of vital importance that we understand all the sources that produce magnetic variations measured by magnetometers. A ground-based magnetometer station measures variations that arise from two distinct sources: external currents in the ionosphere and magnetosphere and internal induced currents in the solid Earth. While in the solid Earth research it is important to remove the source effects caused by nonuniform ionospheric currents [e.g., Pirjola, 1992], for magnetospheric research it is important to understand how much of the mea-

sured variations actually arise from the external current systems and how much is due to induction effects that depend on the Earth's conductivity structure [Viljanen et al., 1995]. Under idealized conditions, the contribution from magnetospheric and ionospheric sources to the magnetic field can be represented by a vertically propagating plane wave; in which case the external and internal parts of the horizontal field are equal. This large value underlines the importance to evaluate the induction effects in the magnetic recordings used in space physics, in particular in the auroral electrojet indices.

The effects of induced currents depend on the Earth's conductivity structure, on the temporal and spatial structure of the ionospheric current, and on the location of the measurement point relative to the source current [Mareschal, 1986]. While horizontal variations in the conductivity structure are difficult to account for, most studies have used layered Earth models thus including variations in the vertical direction only. The number of layers with different conductivity values can range from two up to, for example, seven as used in the model for southern Finland [e.g., Viljanen et al., 1999a]. The largest inductive effects are caused by ionospheric current systems that involve rapid time variations, such as the westward traveling surge during substorms or sudden impulses preceding geomagnetic storms [Viljanen et al., 1999b]. Typically, the inductive effects on  $X$  are largest far away from the source current, where the entire signal is already small [Viljanen et al., 1995]. Near the electrojet it is expected that the inductive effects are particularly important during situations with rapidly changing current systems (such as substorms) and in areas where the Earth's conductivity is high. When the measurements are made at a location far away from the source current, the relative induction contribution to  $X$  is larger for smaller Earth conductivity and is large for slow variations.

The magnetic field separation into external and internal parts in Fennoscandia was first performed by Küppers et al. [1979] and Mersmann et al. [1979] who used data from the Scandinavian Magnetometer Array and applied the traditional one-dimensional separation technique assuming two-dimensionality of the current systems. Later, Richmond and Baumjohann [1984] applied a method that allowed for a full two-dimensional separation for a three-dimensional current system. All these investigations dealt only with single time-step instantaneous field configurations. A more systematic study was conducted by Viljanen et al. [1995], who considered several electrojet events using the IMAGE magnetometer network data. They concluded that the external contribution to the horizontal field close to auroral currents was 70-90%, and even smaller for larger distances from the currents.

In this paper, we examine the inductive effects on the local auroral electrojet indices  $IU$  and  $IL$  created using data from the IMAGE magnetometer network extending from  $56^\circ$  to  $75^\circ$  geomagnetic latitude, from southern

Finland to Svalbard [Syrjäsuo et al., 1998]. In section 2, we expand on the work of Viljanen et al. [1995] to use the Siebert-Kertz formulation [Weaver, 1964] to 77 substorm events recorded by the IMAGE magnetometers during 1997 [Kallio et al., 2000]. For each event separately, each lasting for several hours, we evaluate the internal and external parts of  $IL$ . In section 3, we evaluate the effects of the Earth's conductivity, the effects of the timescales of the variation, and the effects of the scale size of the electrojet using layered Earth models. Furthermore, we discuss time-dependent electrojets and, as a special case, the westward traveling surge as an example of a complex, localized, moving, and temporally changing structure [Amm, 1995; Viljanen et al., 1999b]. In section 4, we summarize the results, discuss the importance of the induction effects during each of the substorm phases, and give some general estimates of the induction effects under several typical ionospheric conditions.

## 2. Separation of Magnetic Variations Into External and Internal Parts

### 2.1. Integrals for Separation

The magnetic variation field observed at the Earth's surface can always be given as the sum of contributions from external (ionospheric and magnetospheric currents) sources and internal sources (induced currents in the Earth). Between the Earth and the ionosphere the magnetic field can be assumed curl-free because the air is poorly conducting and the geomagnetic variations are slow. Consequently, in the air the magnetic field  $\mathbf{B}(\mathbf{r})$  can be expressed as a gradient of a scalar potential  $V(\mathbf{r})$ . Because the magnetic field is always divergence-free, the scalar potential satisfies the Laplace equation

$$\nabla^2 V(\mathbf{r}) = 0. \quad (1)$$

The standard method for solving this equation is to use a spatial Fourier transform. In the following it is assumed that the total magnetic variation field has only  $X$  (horizontal) and  $Z$  (vertical) components ( $\mathbf{B} = X\mathbf{e}_x + Z\mathbf{e}_z$ ) and that the field is independent of  $y$ . It is implicitly assumed that the Earth has a layered structure. The external and internal parts of the field at the Earth's surface can be given in the wave number domain as [e.g., Weaver, 1964]

$$\begin{aligned} \hat{X}_{\text{ext}}(k) &= \frac{1}{2}[(\hat{X}(k) + \text{sgn}(k)\hat{Z}(k))] \\ \hat{X}_{\text{int}}(k) &= \frac{1}{2}[(\hat{X}(k) - \text{sgn}(k)\hat{Z}(k))] \\ \hat{Z}_{\text{ext}}(k) &= \frac{1}{2}[(\hat{Z}(k) - \text{sgn}(k)\hat{X}(k))] \\ \hat{Z}_{\text{int}}(k) &= \frac{1}{2}[(\hat{X}(k) + \text{sgn}(k)\hat{Z}(k)), \end{aligned} \quad (2)$$

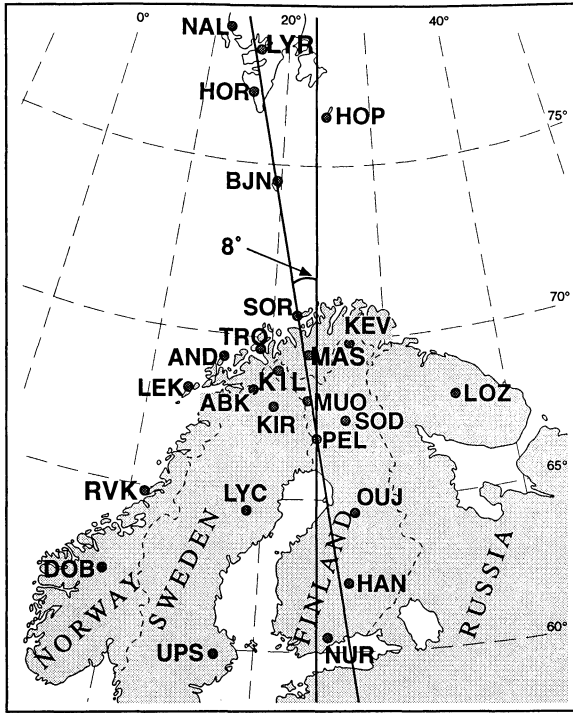


**Figure 1.** IMAGE stations in the chain Nurmijärvi (NUR) - Ny Ålesund (NAL) marked as black dots.

where the Fourier transform  $\hat{f}(k)$  of a function  $f(x)$  is given by

$$\hat{f}(k) = \frac{1}{\sqrt{2\pi}} \int_{-\infty}^{\infty} dx e^{ikx} f(x). \quad (3)$$

The inverse transform yields the separation integrals

$$\begin{aligned} X_{\text{ext}} &= \frac{1}{2}(X + KZ) \\ X_{\text{int}} &= \frac{1}{2}(X - KZ) \\ Z_{\text{ext}} &= \frac{1}{2}(Z - KX) \\ Z_{\text{int}} &= \frac{1}{2}(Z + KX), \end{aligned} \quad (4)$$

where  $K$  is an operator defined by

$$Kf(x) = \frac{1}{\pi} \int_{-\infty}^{\infty} du \frac{f(u)}{x-u} \quad (5)$$

Equation 4 directly shows that for the plane wave case, i.e.,  $Z = 0$ ,  $X_{\text{ext}}$  and  $X_{\text{int}}$  are equal and 50% of  $X$ . Analogous separation formulas can also be given for the general case where the magnetic field depends on all three spatial coordinates. However, the magnetic field then needs to be known everywhere at the Earth's surface, which is not the case in this study.

We utilize data from 11 IMAGE stations in the chain Nurmijärvi (NUR) - Ny Ålesund (NAL) marked with black dots in Figure 1. The  $x$  axis is rotated  $8^\circ$  westward to get approximately a magnetic meridian line (crossing station PEL for which geogr.lat =  $66.90^\circ$ , and

geogr.long =  $24.08^\circ$ ). In the rotated frame,  $B_N$  and  $B_E$  mark the north and east components of the magnetic field.

The integral in (5) has a singularity at the observation point  $x$ . However, assuming that the function  $f$  varies linearly between observation points, the singularity can be removed [Schmucker, 1970]. The end points of the chain are also somewhat problematic: To avoid sharp jumps at the ends, we extrapolated the field 150 km out of the chain by assuming that  $X$  decays as  $x^{-2}$  and  $Z$  as  $x^{-3}$ . Such an asymptotic behavior is valid for a line current if the Earth's conductivity is uniform [Viljanen et al., 1995]. For values in the middle of the chain the form of the field continuation is not important. Details of the numerical computation of (5) are given in the appendix A.

The method was tested by calculating the field caused by a line current flowing at altitude  $h$  above the  $y$  axis. The induction effects were taken into account by setting a perfect conductor at depth  $d$ . Then the total field at the Earth's surface is the sum of the fields due to currents at  $z = -h$  and  $z = h + 2d$ . For a sheet current at the ionospheric altitude ( $\sim 100$  km) values of some hundred kilometers were used for  $h$  (see section 3.1.). The separation was performed using (4) and the modeled field values at the 11 IMAGE stations. To get an equivalent of an  $IL$  index, the field was evaluated at the point where  $X$  had its minimum. Comparisons of the ratio of the external part to the total field showed a good agreement between analytically calculated and numerically separated values. However, at the  $IL$  site, there seems to be a small systematic error caused by the calculation of the integral in (5), which makes the ratio some percent units too small. The largest errors occur at Bear Island (BJN), which is the most isolated site. These conclusions are valid also in the case of two line currents having different amplitudes, locations, and heights.

One important problem is that the real field always depends on all three spatial coordinates. Thus the validity of the assumption of the two dimensionality must be carefully evaluated for each event separately. Earlier, an experimental test was carried out by Richmond and Baumjohann et al. [1984], who separated a three-dimensional field recorded by the Scandinavian Magnetometer Array. They found the differences between one-dimensional and two-dimensional separations negligible even when the field had substantial variations in all three dimensions. The differences were comparable to the inherent mapping errors in their optimal linear estimation technique. Similarly, Küppers et al. [1979] separated the field along two parallel chains of SMA and found a negligible difference for a case with an eastward electrojet.

The Siebert-Kertz separation of the field can be used for magnetic data either in the time domain or in the frequency domain [Weaver, 1964]. The separation formulas also show that once  $X$  and  $Z$  are known, the ex-

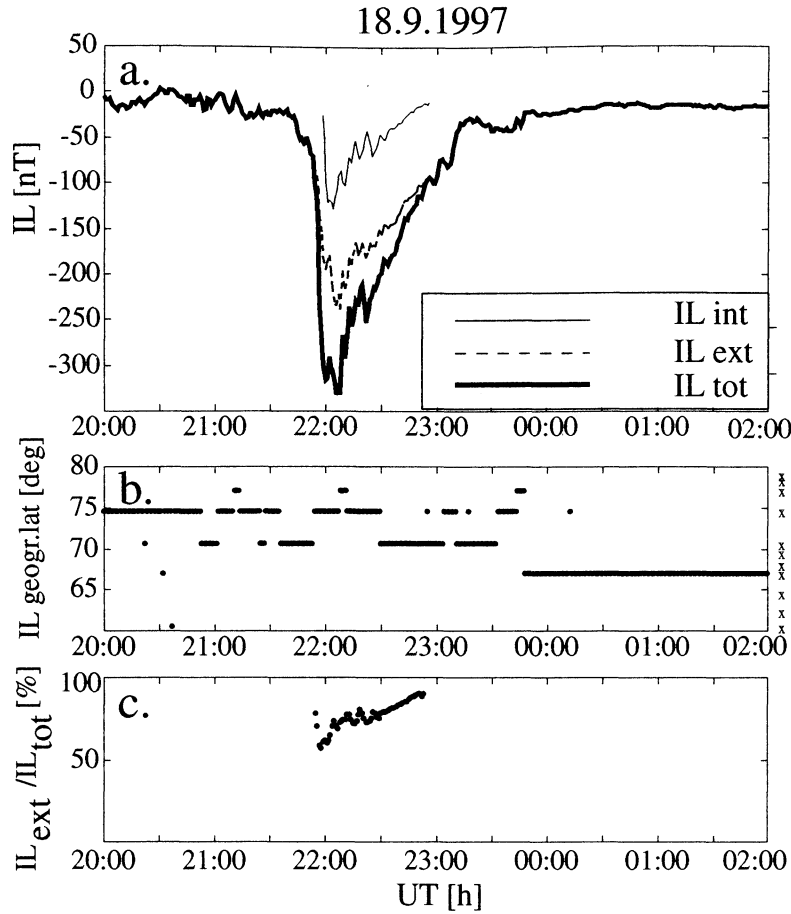


**Figure 2.** Sample event September, 18, 1997: (a)  $IL_{tot}$ ,  $IL_{ext}$  and  $IL_{int}$ , (b) geographical latitude of the station contributing to the  $IL_{tot}$  and (c)  $IL_{ext}/IL_{tot}$ .

ternal and internal contributions to these components are uniquely determined. For example,  $KZ$  and  $X$  always give the difference and the sum of the external and internal parts of  $X$ , respectively, thus permitting a unique solution of  $X_{ext}$  and  $X_{int}$ .

When time (or frequency) does not appear explicitly in the separation formulas, a question may arise how the temporal variations affect the magnitude of the internal contribution to the surface fields. Physically, a fast time variation of the external magnetic field induces an intense electric field, which results in large ohmic currents in the Earth and, consequently, in a larger induced magnetic field. In addition, a rapid variation decreases the skin depth in the Earth and thus implies that the ground currents are located closer to the surface. In the mathematical separation formulas, the magnitude and location of the induced currents have an influence on the spatial distributions of  $X$  and  $Z$ , thus affecting the values of  $KX$  and  $KZ$ . In other words, the separation equations automatically account for the effects of temporal changes. This occurs via the contributions of  $X_{int}$  and  $Z_{int}$  to  $X$  and  $Z$  while  $X_{ext}$  and  $Z_{ext}$  only depend on the instantaneous ionospheric-magnetospheric current distribution.

## 2.2. Application to IMAGE Data

The formulas above present a way to determine the external and internal contributions of recorded geomagnetic variations without any prior knowledge of the subsurface geological structure or of the ionospheric currents (provided the assumption of a two-dimensional situation can be made). In this section, the external and internal contributions to the locally derived auroral electrojet index  $IL$  are examined for 77 substorms. These events were selected from a data set compiled of all substorms during 1997 that occurred while the IMAGE magnetometer chain was in the night sector [Kallio *et al.*, 2000]. In this statistic, only relatively isolated substorms, where the onsets could be clearly defined, were accepted. For each substorm separately, the internal and external contributions at each station were derived using the Siebert-Kertz formulation presented in section 2.1. Following that the regular  $IL$  index was separated into external and internal parts which gives two new indices  $IL_{ext}$  and  $IL_{int}$ .

Figure 2a shows the  $IL$  index during a substorm on September 18, 1997, during 2000–0200 UT (thick solid line). The thin solid line shows the external contribution, i.e., the response to the ionospheric currents. The

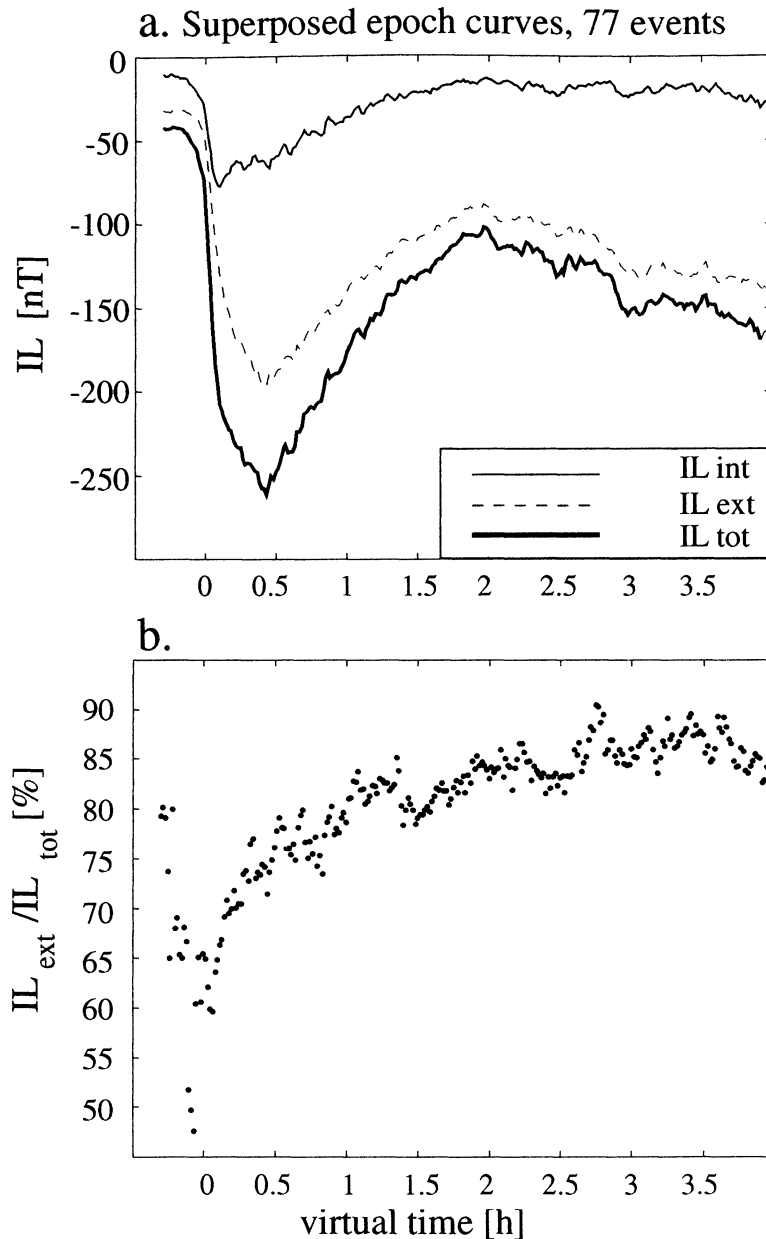


**Figure 3.** The results for the 77 substorms during 1997 in the form of a superposed epoch analysis (a) for  $IL_{tot}$  and (b) for ratio  $IL_{ext}/IL_{tot}$ .

thick dotted line shows the internal contribution arising from subsurface currents. The internal contribution peaks strongly at substorm onset and then decays over a time period of  $\sim 30$  min. This is a typical feature seen in almost every substorm event. Notice also that the internal currents contribute  $\sim 40\%$  to the maximum  $IL$  value and that it also substantially increases the time derivative at substorm onset. This makes the intensification seem much more rapidly evolving in time than the external disturbance actually does.

Figure 2b shows the geographic latitude of the magnetometer station contributing to the  $IL$  index as a function of time. The main contribution comes from stations at relatively high latitudes, mostly from Bear Island at  $75^\circ$ . This is another typical feature of the

data set analyzed here. Figure 2c shows the ratio of the external field to the total field ( $IL_{ext}/IL_{tot}$ ). Here, as in Figure 2a, only values where the current system was judged to be sufficiently two-dimensional (using the criterion  $B_E/B_N < 50\%$ ) were plotted. This representation clearly shows how the external contribution at substorm onset is  $\sim 60\%$  of the total field and how it almost linearly increases to near the quiet time value of 80–90%.

The results for the 77 substorms are presented in Figure 3a in the form of a superposed epoch analysis, centered around the substorm onset time. The results demonstrated in the previous example are clearly reproduced here: the internal contribution maximizes shortly after the substorm onset and contributes to a larger

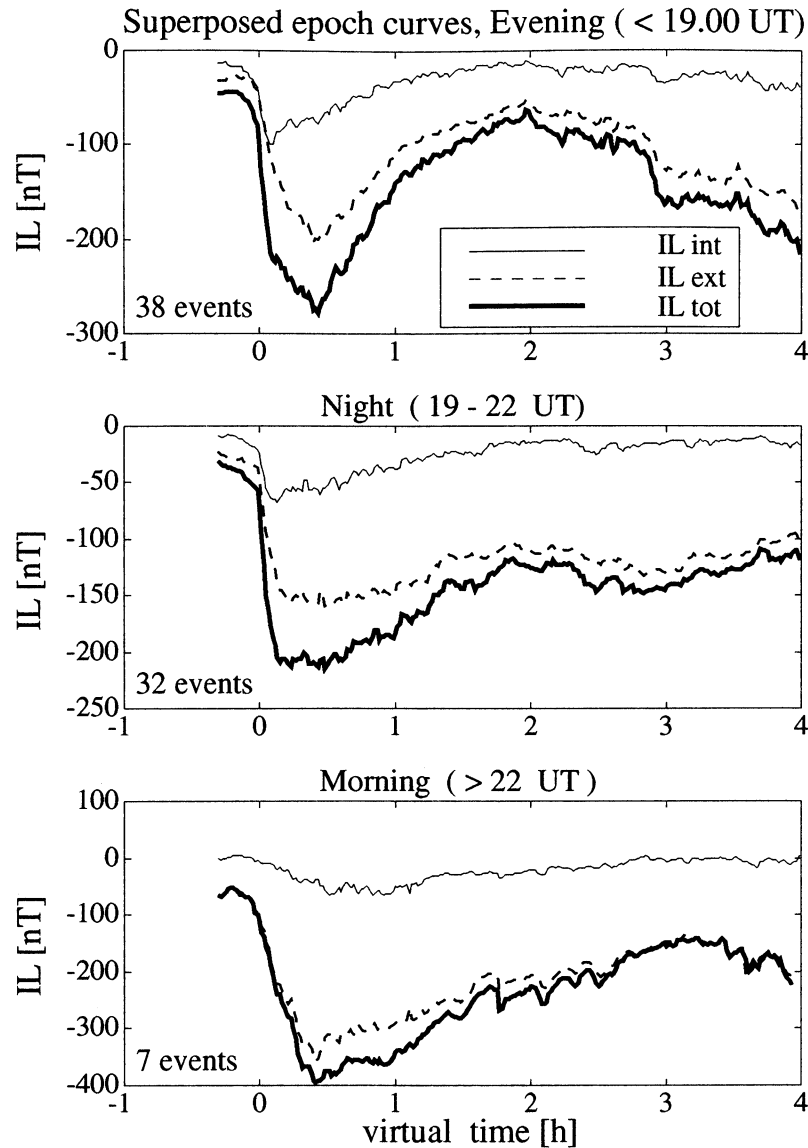


**Figure 4.** The results for the 77 substorms during 1997 in the form of a superposed epoch analysis for different time sectors.

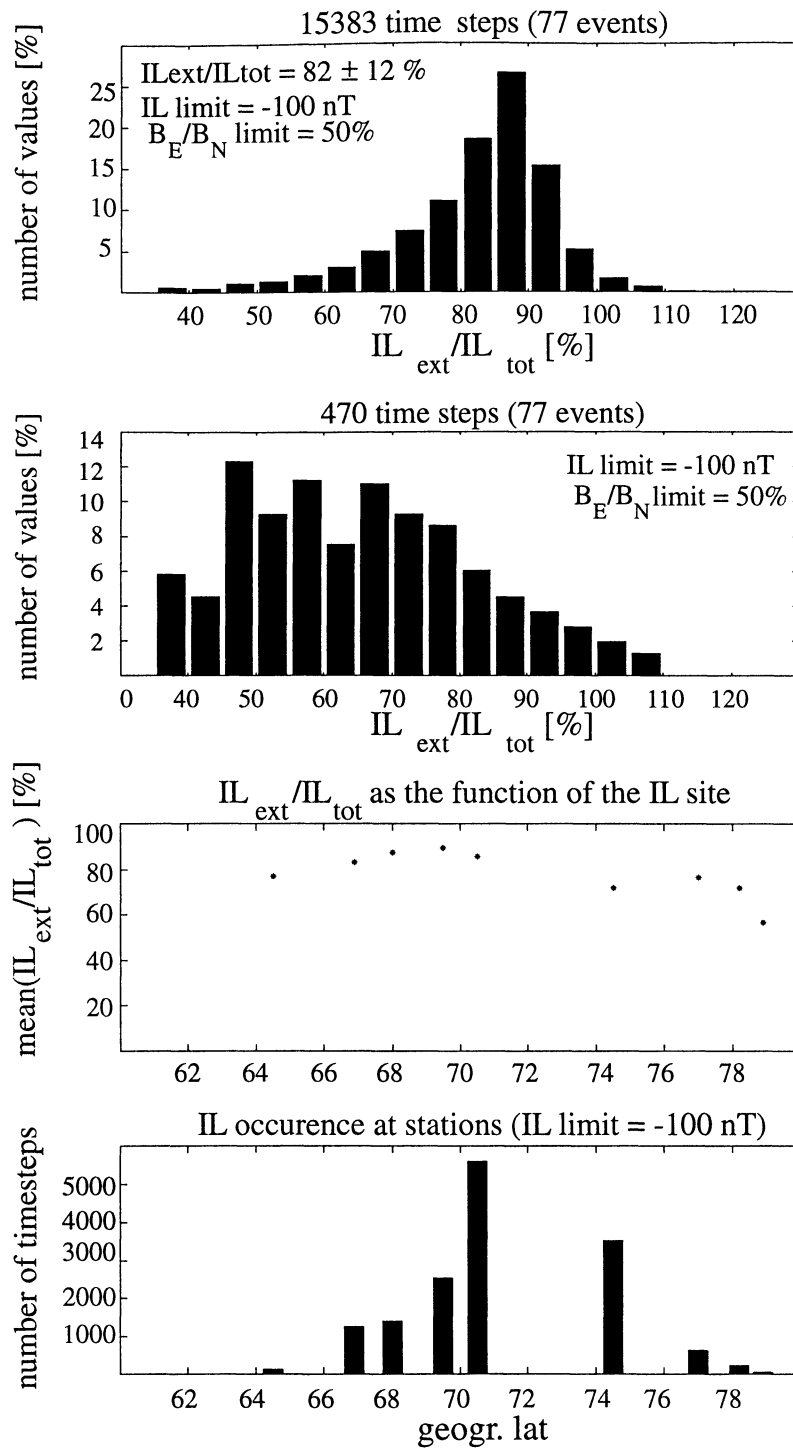
$IL_{\max}$  and a more rapid decrease of the  $IL$  index. Figure 3b shows  $IL_{\text{ext}}/IL_{\text{tot}}$  values so that zero marks the substorm onset time. During onset time the ratio varies between 60 and 65%.

Figure 4 shows the same superposed epoch analysis results, but now the events are divided into three local time sectors. The evening sector covers substorm onset times before  $MLT = 2130$ , the night sector contains the local times  $2130 < MLT < 0030$ , and the morning sector substorms occur after  $MLT = 0030$ . The results show that the induction effects are strongest for the evening sector, where the effect to the  $IL$  index time derivative is the largest. In the midnight sector, the induction effects are also substantial and maximize promptly after the substorm onset. However, for the morning sector substorms, the induction effects are small, and their contribution to the index actually maximizes only after the peak of the substorm intensity. This can be explained

by the fact that the most localized and strongest currents are associated with the westward traveling surge in the evening sector. Therefore, in the morning sector, relatively small effects are seen in the induction component until the substorm recovery phase.

In a statistical sense, Figure 5a shows the distribution of the external to total disturbance ratios ( $IL_{\text{ext}}/IL_{\text{tot}}$ ) for 6-hour periods around the 77 substorm events. This shows that averaged over time, the external contribution is close to 90% of the total field and that for two thirds of the time the external field is more than 80% of the total field. However, there is a substantial tail in the distribution toward lower external field contributions, which, as demonstrated previously, comes from near the maximum disturbances or near the substorm onset times. At the other end of the distribution, there are values exceeding 100%.

If we concentrate on the first 10 min of the expansion



**Figure 5.** The distribution of the external to total disturbance ratio  $IL_{ext}/IL_{tot}$  for (a) the 6-hour period and (b) the first 15 min of the expansion phase around the 77 substorm events. (c) Latitudinal variation of  $IL_{ext}/IL_{tot}$ . (d) The number of time steps recorded at each station.

phase during each substorm, the picture is substantially changed (Figure 5b). At substorm onset, close to the minimum- $IL$  time, the external contribution is on average  $\sim 60\%$  of the disturbance, and some very low values are observed. The differences between Figures 5a and 5b outline the fact that the induction effects are largest during the times of rapid changes, and are important enough to be included in studies examining substorm

onsets and disturbance sizes using the electrojet indices.

In order to examine the latitudinal variation of the induction effects, Figure 5c shows the average external to total field contributions for each station separately, ordered in geographic latitude. It can be seen that the stations located over the Arctic Ocean (above  $70^\circ$ ) show smaller values of this ratio and hence larger induction effects. The difference between the mainland and island

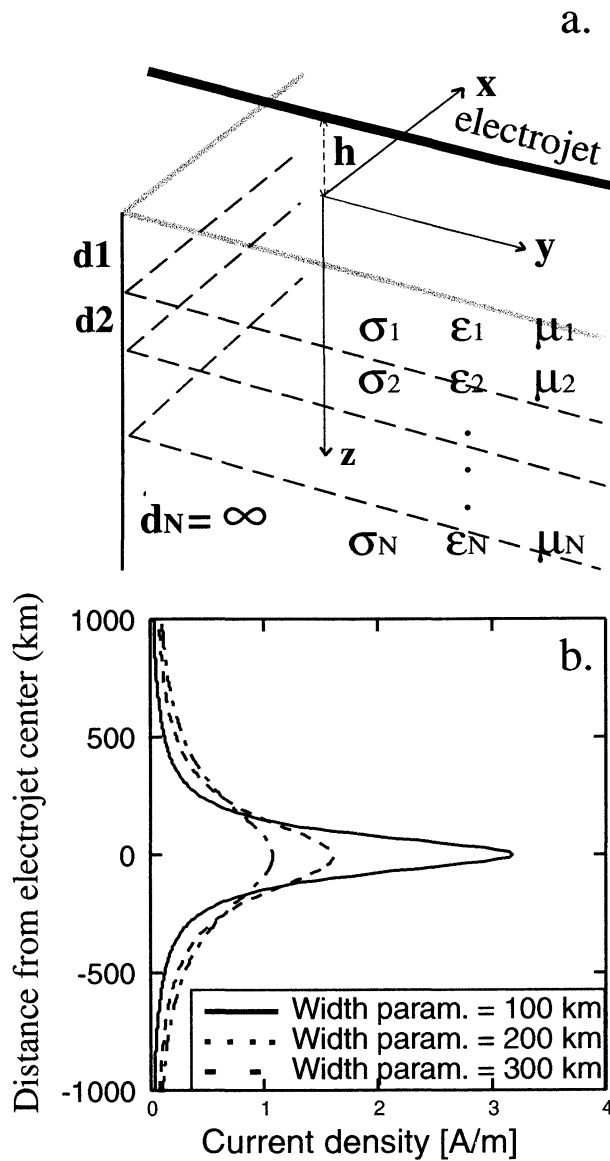


**Figure 6.** (a) Line current electrojet located at height  $h$  above a layered Earth. (b) The current density as a function of  $x$  for different values of the width parameter  $L$  when the total current in the electrojet equals 1 MA.

stations is  $\sim 10\%$ . For reference, Figure 5d shows the number of time steps recorded at each of the stations. The distribution peaks strongly between  $70^\circ$  and  $75^\circ$ ; however, except for the southernmost and northernmost stations, the statistical coverage is good.

### 3. Physical Interpretation

#### 3.1. Line Current Model

The simplest model for an auroral electrojet is an east-west directed line current  $J$  located at an altitude  $h$  above the Earth's surface (Figure 6a). The Earth is assumed to have a layered structure in which each layer is characterized by thickness  $d_i$ , conductivity  $\sigma_i$ , permeability  $\mu_i$ , and permittivity  $\epsilon_i$ . A single frequency  $\omega$  is considered, i.e., the time dependence is of the form

$\exp(i\omega t)$ . The electric and magnetic fields at the Earth's surface arise primarily from the line current and secondarily from currents induced in the Earth. These fields can be calculated from Maxwell's equations using boundary conditions which result in inverse Fourier integrals over the horizontal wave number [Hermann and Peltier, 1970]. For an infinitely long line current the electric field has only one component ( $E_y$ ) parallel to the line current, and the magnetic field disturbance in the  $y$  direction is zero. The use of the line current model allows for addressing the fundamental principles associated with the induction contribution.

More realistically, the electrojet is a sheet current with a nonzero width in the  $x$  direction (Figure 6b). If the current distribution in the sheet at height  $h$  is of the Lorentzian form

$$j(x) = \frac{JL}{\pi(x^2 + L^2)}, \quad (6)$$

where  $L$  is a width parameter, the electric and magnetic fields produced at the Earth's surface are the same as those produced by a line current  $J$  at the height  $h + L$  [Maurer and Theile, 1978]. Thus the line current is equivalent to a lower-altitude sheet current with a Lorentzian profile.

Electric and magnetic fields for any sheet current distribution are also easily obtained by a superposition of the line currents. Häkkinen and Pirjola [1986] present formulas for the surface fields produced by a general electrojet current supplemented by field-aligned currents. Numerical computations can be simplified by applying a complex image method (CIM), in which the Earth is (approximately but to a high accuracy) replaced by a perfect conductor located at a complex depth [Pirjola and Viljanen, 1998].

In the numerical computations, it is assumed now that  $h = 110$  km and  $J = 1$  MA. The periods  $T = 2\pi/\omega$  range from 1 min (corresponding to a rapid change) to 1 hour (corresponding to a slow variation during a substorm). The width parameter  $L$  ranges from 0 to 300 km. Three layered Earth models are discussed: (1) A highly conducting land area with layer thicknesses 3, 6, 5, 7, 23, 106, and  $\infty$  km, and resistivities 5000, 500, 100, 10, 20, 1000, and  $1 \Omega\text{m}$  is discussed. This model is roughly valid for southern Finland [Viljanen et al., 1999a]. (2) A poorly conducting land area with layer thicknesses 12, 22, 16, 50, 50, and  $\infty$  km, and resistivities 30000, 3000, 50, 1000, 5000, and  $1 \Omega\text{m}$  is discussed. This model is roughly valid for central Finland [Viljanen et al., 1999a]. (3) A simplified ocean model (including the basement below the seawater) with layer thicknesses 1, 149, and  $\infty$  km, and resistivities 0.25, 100, and  $1 \Omega\text{m}$  [Heinson and Constable, 1992] is also discussed. The permeabilities are set equal to the vacuum value. Owing to low frequencies, permittivities do not play any role in practice.

In the mathematical treatment the field quantities are complex numbers with their absolute values and phases

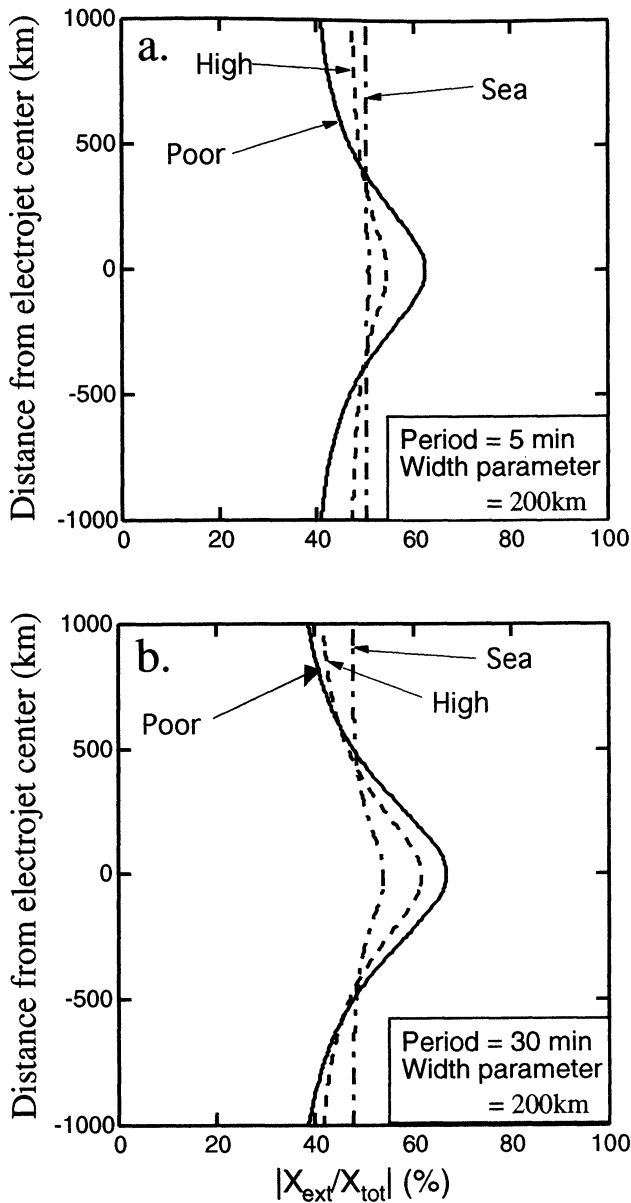


**Figure 7.** The absolute values of the ratio of the external part to the total  $x$  component for the periods (a)  $T = 5$  min, and (b)  $T = 30$  min. The electrojet width parameter equals 200 km

giving the amplitudes and the phase differences with respect to the primary source. The ratios of the primary and induced parts of  $X$  to the total  $X$  component are thus also complex and, to obtain the relation between the amplitudes, the absolute values of the ratio are considered.

**3.2. Effect of the Earth's conductivity**

The induction contribution to surface fields depends on the conductivity structure of the Earth. We now consider the three layered models presented in section 3.1 and set the electrojet width parameter  $L$  equal to 200 km.

Figures 7a and 7b depict the absolute values of the ratio of the external part to the total value of the mag-

netic  $X$  component as functions of the  $x$  coordinate for periods  $T = 5$  min and  $T = 30$  min, respectively. The results show that the dependence of the ratio on  $x$  becomes more pronounced as the conductivity decreases. This conclusion is obviously equivalent with the well-known fact in magnetotellurics that source effects decrease with an increasing conductivity [Viljanen et al., 1999a]. For the sea model, the ratio is very accurately 50% everywhere; this is actually the plane wave result (see section 2.1). The general behavior of the ratio is the same for  $T = 5$  min and  $T = 30$  min, but the variation with  $x$  is larger for the longer period. In each case the ratio is at maximum just below the center of the electrojet, ranging between 55 and 70% for the high and poor Earth conductivities.

Far away from the electrojet, the ratio is smallest for the lowest conductivity model, being only  $\sim 40\%$ . It is also important to note that the limit value of the ratio at large  $x$  values does not equal the plane wave result of 50%. However, at large distances all contributions to  $X$  are small, as shown in Figure 8, which presents the real and imaginary parts of  $X$ ,  $X_{ext}$ , and  $X_{int}$  for  $T = 5$  min and  $L = 200$  km and for the highly conducting Earth structure.

**3.3. Effect of the Period**

The external contribution to the magnetic field does not depend on the period, as it is obtained from the Biot-Savart formula independent of  $\omega$ . Figures 7a and 7b, however, present a clear effect of the period. This results naturally from the fact that the induced electric field, which drives currents within the Earth, depends on the rate of change of magnetic variations. We now

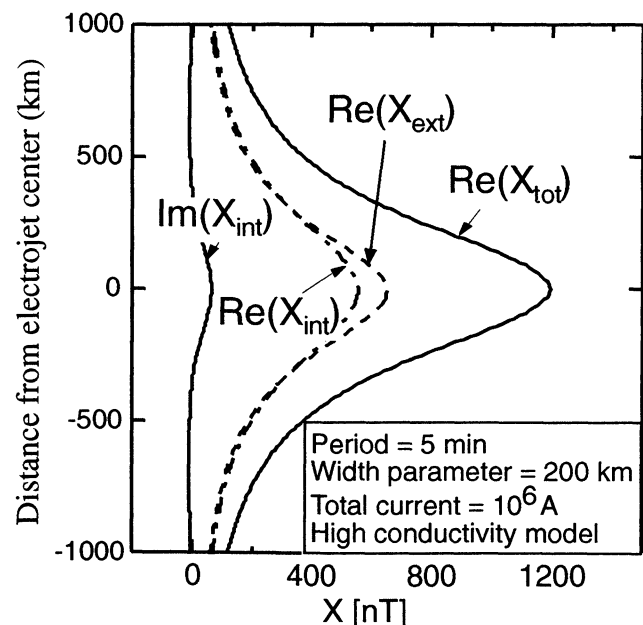


**Figure 8.** The real and imaginary parts of  $X$ ,  $X_{ext}$  and  $X_{int}$  for  $T = 5$  min and  $L = 200$  km. The Earth has the highly conducting structure labeled "High" in Figure 7

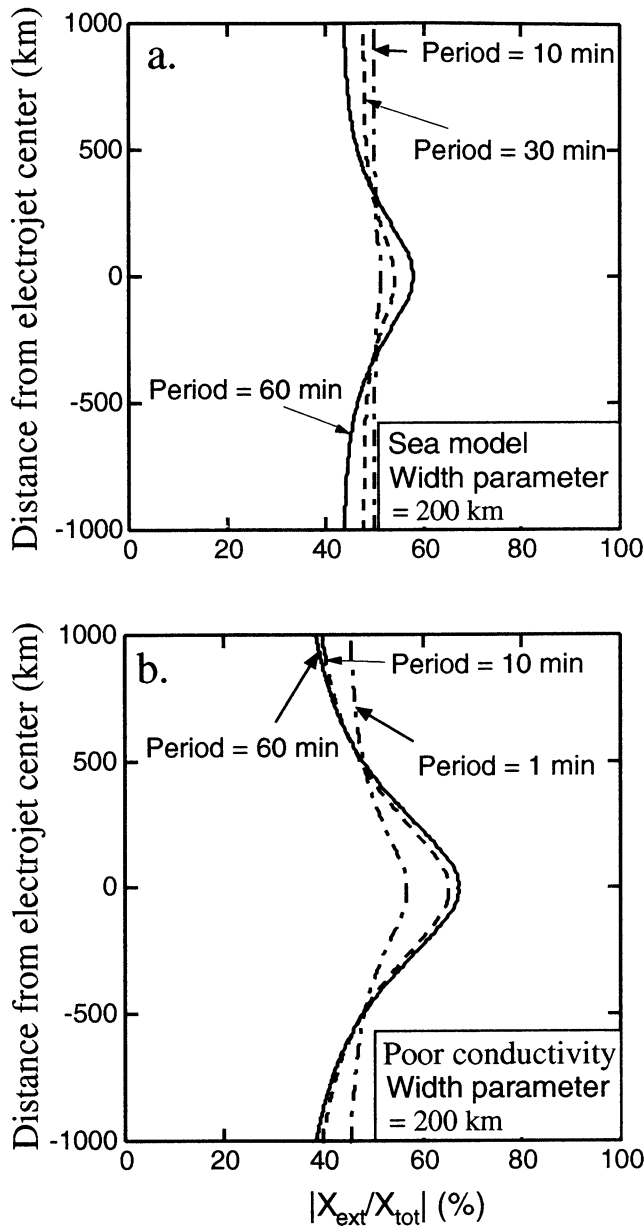


**Figure 9.** The absolute values of the ratio of the external part to the total  $X$  component for different periods and for (a) the ocean conductivity model and (b) the poorly conducting Earth model. The electrojet width parameter equals 200 km.

consider the periods  $T = 1, 10, 30, 60$  min and, as in section 3.2, set the electrojet width parameter  $L$  equal to 200 km.

Figures 9a and 9b depict the absolute values of the ratio of the external part to the total value of the magnetic  $X$  component as functions of the  $x$  coordinate for the ocean conductivity and poorly conducting structures, respectively. In Figure 9a, the curve for  $T = 1$  min is not plotted because it very exactly follows the result for  $T = 10$  min. Similarly, the curve for  $T = 30$  min is practically equal to the case for  $T = 60$  min in Figure 9b. These figures support the previous conclusion that an increase of the period makes the ratio more dependent on  $x$ . This is again a conclusion which is equivalent with

the well-known fact in magnetotellurics that source effects increase with an increasing period [Viljanen *et al.*, 1999a].

For the ocean model, the ratios do not differ much from 50% even for  $T = 60$  min. The general behavior of the ratios is the same for the two conductivity models, but as in Figure 7, the variation with  $x$  is larger for the less conducting case.

### 3.4. Effect of the Width of the Electrojet

The width of the electrojet also affects the magnitudes of the different contributions to  $X$ . In the extreme

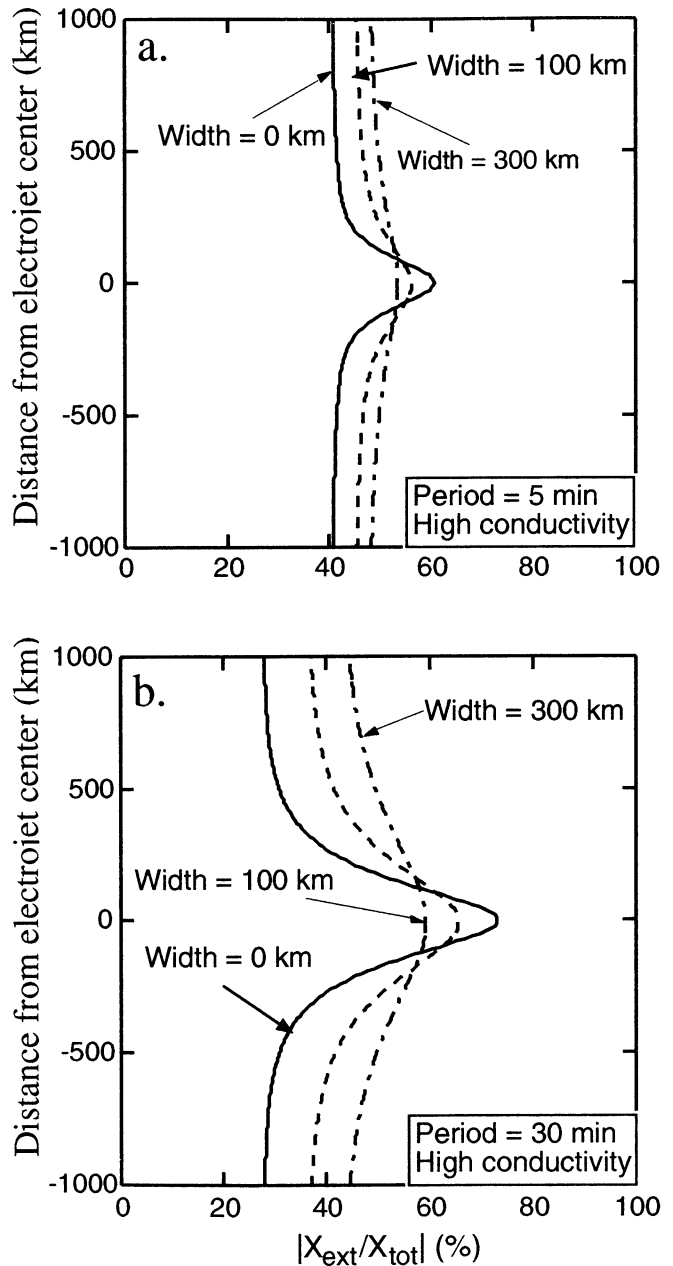


**Figure 10.** The absolute values of the ratio of the external part to the total  $X$  component for different values of the electrojet width parameter and for periods  $T = 5$  min and  $T = 30$  min. The Earth has the highly conducting structure.

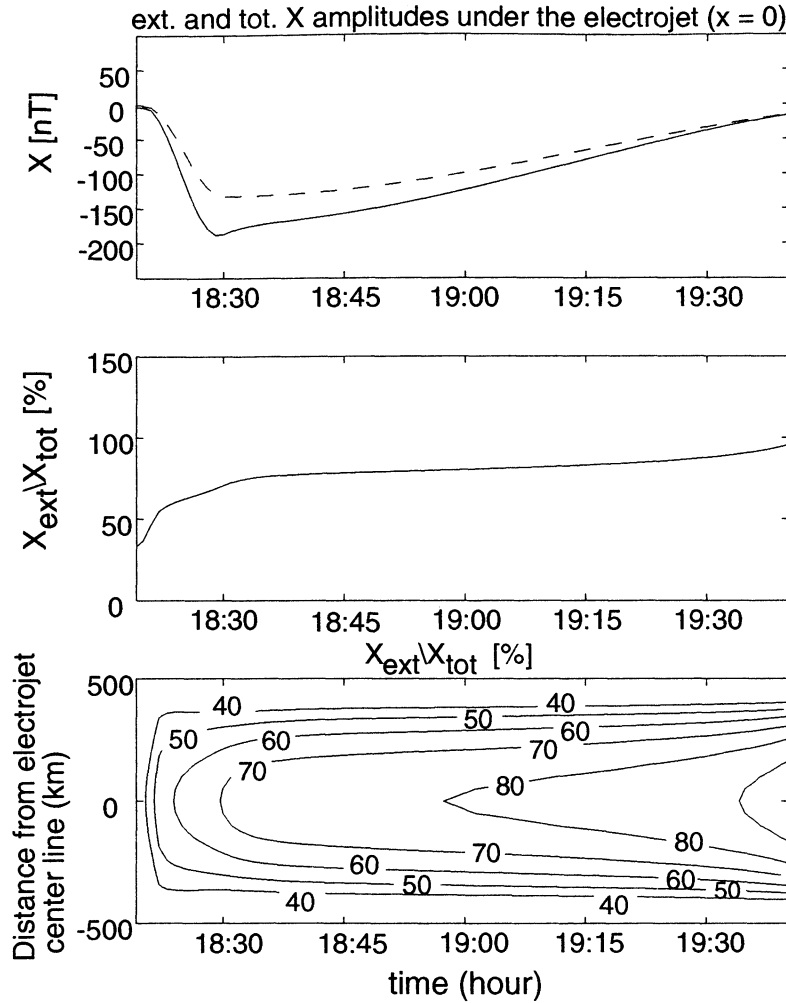


**Figure 11.** top) external and total  $X$  under the center of an electrojet of a horizontal length of 1000 km and having vertical currents at the ends. The horizontal current flows at a height of 300 km and has a time-dependence that smoothly follows  $IL$  in Figure 2a. (middle) External to total  $X$  ratio under the electrojet. (bottom) External to total ratio of the  $X$  component of the magnetic field as a function of time and  $x$  coordinate. The conductive Earth model is used.

case of an infinite sheet current the fields are vertically propagating plane waves, and then the external and internal parts of  $X$  are equal. Figure 6b shows the current density as a function of  $x$  for different values of the width parameter  $L$  when the total current in the electrojet equals 1 MA.

We consider the highly conducting Earth structure and electrojet width parameter values  $L = 0, 100, 300$  km. Figure 10 depicts the absolute values of the ratio of the external part to the total value of the magnetic  $X$  component as functions of the  $x$  coordinate for the periods  $T = 5$  min and  $T = 30$  min, respectively. It is seen that the dependence of the ratio on  $x$  is larger for a narrow electrojet, which is in agreement with the observation that magnetotelluric source effects are strong for localized ionospheric sources. In the extreme case of a line current ( $L = 0$ ), the ratio varies between  $\sim 30$  and 70% for different  $x$  values when  $T = 30$  min.

### 3.5. Time-Dependent Electrojet

As seen in section 2.3, the internal contribution is rel-

atively largest near the substorm onset time. A qualitative explanation is that then small periods have a larger effect than during the recovery phase. As shown in section 3.2 and 3.3, the induction effects under an electrojet are most significant at small periods.

In this section, we study the phenomenon quantitatively by calculating analytically the external and internal field by the complex image method whose application in time-domain problems is demonstrated by *Viljanen et al.* [1999b]. We consider an east-west line current at a height of 300 km. The length of the horizontal part of the current is 1000 km (from  $y = -500$  km to  $y = 500$  km), and the ends of the electrojet are connected to vertical (field-aligned) currents that flow to and from infinity. The amplitude of the electrojet is assumed to follow smoothly the shape of the total  $IL$  in Figure 2a. We use the conductive Earth model. The calculated ratio of the external to the total  $X$  under the electrojet along the profile  $y=0$  ( $=IL$ ) is shown in Figure 11. We also used the resistive Earth model and obtained nearly an identical result.

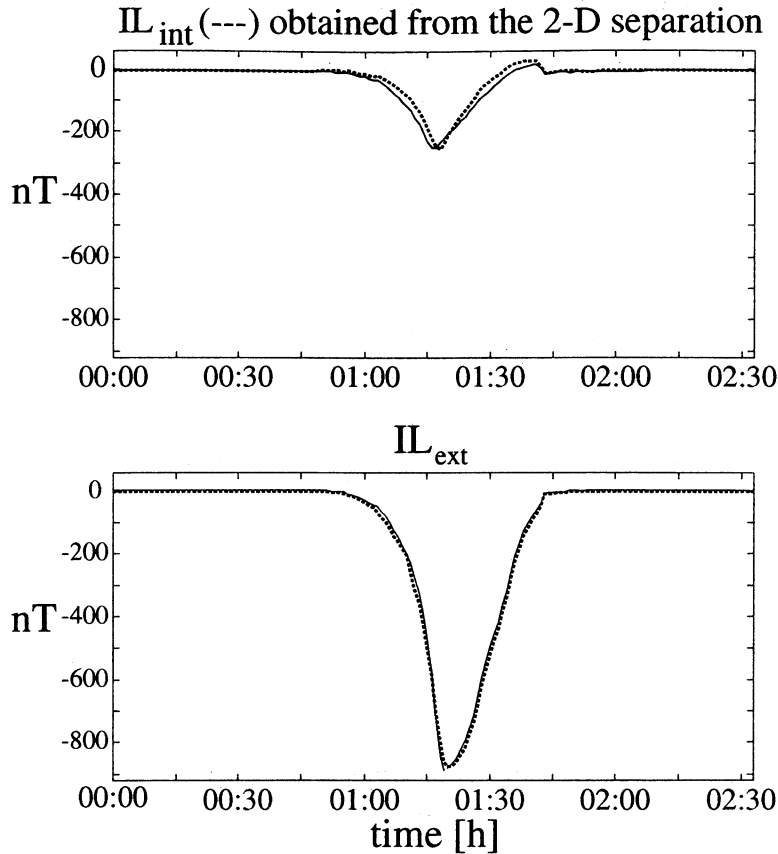


**Figure 12.** Exact (uniform line) and one-dimensionally separated (dashed line)  $IL$  when a westward traveling surge (WTS) is considered. The velocity of WTS is 1 km/s and its center approximately crosses the IMAGE station Muonio (MUO). The conductive Earth model is used.

Under the electrojet (at the  $IL$  station) the ratio of the external to total  $X$  has the same basic feature as observed in section 2.2: at onset it has a minimum, and then it gradually approaches 100%. This is in agreement with the frequency consideration: near the onset time high frequencies are more dominating than at other times which increases the internal contribution.

### 3.6. Two-Dimensional Modeling of the Westward Traveling Surge

The results presented in this paper are based on the one-dimensional separation technique presented in section 2.1. To justify this approach, we now consider a realistic three-dimensional model of a westward traveling surge (WTS) given by *Amm* [1995]. The WTS model is of a specific interest because the largest induction effect occurs at the onset time, and WTS is expected to be a reasonable current model then. We calculate the time-dependent total magnetic field at the Earth's surface with the complex image method whose application to the WTS case is explained by *Viljanen et al.* [1999b]. The field is calculated at the 11 IMAGE magnetometer stations used in this work (Figure 1). The calculated total field is the input to the one-dimensional separation routine, and the external part is compared to that obtained directly by the Biot-Savart law.

The resistive and conductive Earth models are used as previously. We let the WTS to cross the IMAGE chain at three locations: above Muonio (MUO), Bear Island (BJN), and Ny Ålesund (NAL). The velocity of WTS is 1 km/s or 5 km/s, the second value corresponding to quite an intensive event. The (one dimensionally) separated and directly calculated external and internal parts of  $IL$  are compared in Figure 12, where WTS approximately crosses MUO and moves with the velocity of 1 km/s, and the highly conducting Earth model is assumed. The agreement between the two methods is within a few percent units for both conductivity models and velocities. When WTS crosses BJN, the one-dimensionally separation systematically yields too small external  $IL$ . It follows that as a rule of thumb, the external to total  $IL$  ratio may be even 10% units too small for events occurring above the Arctic Ocean. However, the ratio has the same behavior as for the events above the continent: the smallest value occurs at onset, and the ratio increases during the recovery.

Consequently, the separation results of this paper are reliable even though the geometry of the magnetic field does not fulfill the exact requirements for the one-dimensional approach. When the separation results are inspected at single stations, larger deviations appear, but for our study, only the  $IL$  site is important.

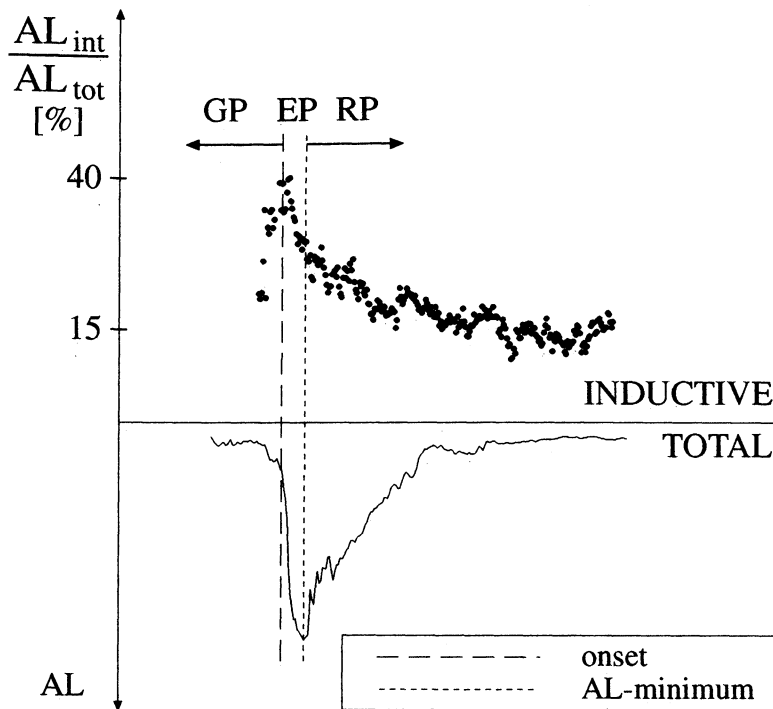


**Figure 13.** The distribution of the external to total disturbance ratio  $IL_{ext}/IL_{tot}$  for different substorm phases.

#### 4. Discussion

In this paper we have examined the separation of magnetometer recordings into two parts, representing the contributions from sources internal and external to the Earth. It is well known that ionospheric currents induce currents within the Earth and that the variations measured by a magnetometer are then a combination of the external and internal contributions [Mareschal, 1986]. The novel results in this paper are the characterization of the internal contribution as a function of the substorm phase. We found that, on average, the internal component is  $\sim 40\%$  of the total field variation around the substorm onset time, while the average value is closer to  $20\%$ . Furthermore, the internal contribution decreases only slowly to the  $20\%$  value such that during much of the expansion phase the internal contribution is between  $20$  and  $40\%$ . Figure 13 shows schematically how the internal contribution rises already slightly before the substorm onset, maximizes during the rapid decrease, and returns to lower values in a quasi-linear manner. This behavior is typical for almost all substorms, while the maximum value of the internal component varies from  $30$  to over  $60\%$ . This study was conducted using the IMAGE meridional magnetometer chain and a local auroral electrojet index  $IL$ . However, the results can be readily generalized to the global  $AL$  index.

The sharp increase of the internal component has two pronounced effects on the shape of typical auroral electrojet ( $AL$ ) curves: it substantially increases the rate of change of the  $AL$  index at substorm onset, and it in-

creases the minimum value (maximum disturbance) by  $40\%$ . These results should be taken into account when the  $AL$  index (or ground magnetometer recordings in general) are used in studies of ionosphere - magnetosphere coupling or ionospheric electrodynamics.

In modeling the substorm-associated ionospheric current system, it is common to use the magnetometers to deduce the ionospheric (equivalent) current pattern and ionospheric radars to deduce the flow or electric field patterns; auroral information can sometimes be used to derive information about the conductivity structure [Oppenorth *et al.*, 1983; Lu *et al.*, 1998]. Using various modeling techniques, the full ionospheric electrodynamics can be deduced [Baumjohann *et al.*, 1981; Amm, 1995; Ridley *et al.*, 1998]. For such studies, it is important to realize that the strengthening of the ionospheric current system is not as rapid as the  $AL$  index or individual magnetograms would suggest and that the total intensity of the currents is only  $60\%$  of the value one obtains by interpreting the magnetic variation as an external current.

The ground-based studies have suggested that the substorm current wedge carries a total current of about  $1$  MA [e.g., Kamide *et al.*, 1981; Oppenorth *et al.*, 1980]. However, empirical modeling results suggest that it is difficult to close such a large current through a localized part of the magnetotail, as the large current tends to change the magnetic topology of the tail [Donovan, 1993]. Furthermore, MHD simulations predict currents in the substorm current wedge that are somewhat smaller, of the order of  $0.1$  MA [e.g., Birn and Hesse, 1991]. If the internal portion is removed from

the ground magnetic records, the ionospheric estimates come closer to those suggested by the magnetospheric studies.

In the second part of the paper (section 3), we examined the physics of the inductive ground currents: effects of the Earth's conductivity, of the temporal variations of the external current system, and of the geometry of the electrojet were all examined separately. A general conclusion was that the induction effects are largest for highly conducting Earth (e.g., seawater) and for high-frequency variations (e.g., substorm onsets). Far away from the electrojet (or other current system) the inductive effects are always large and close to 50%, but there the total field variations are already small. Here we briefly summarize the results concerning the variations below or close to (within 300 km from the center) the current system, where the disturbances are largest.

It is evident from Figure 7 that the higher the ground conductivity, the higher the inductive component is; for ideally conducting Earth the inductive component would be 50% of the total variation. This is significant when measurements from different stations are compared with each other: The variations in the  $X$  components are 20% larger for stations surrounded by oceans compared to inland stations. Thus also the  $X$  components carry substantial information about the geological structure surrounding the magnetometers.

Second, there is a marked increase of the inductive component during times when the current system is rapidly changing in time. Frequency analysis (not shown here) shows that during substorms, the variations are composed of many frequency components such that the fastest variations dominate around the substorm onset time, and during the expansion and recovery phase the dominant frequency slowly decreases. This causes the typical shape of the inductive internal component increasing sharply at substorm onset and decaying during the expansion and recovery phases as depicted in Figure 13. These results suggest that it is not sufficient to correct the magnetogram recordings by a constant value but that the frequency of the external signal needs to be taken into account.

Third, the effects of the scale size of the electrojet were examined. The results show that the inductive effects are largest for large-scale current systems near the electrojet center, whereas strongly localized current systems lead to smaller inductive components near the electrojet center but much larger inductive effects further away. Again, the strong dependence on the geometry of the current system indicates that each case should be evaluated individually.

Finally, we examined the validity of the assumptions made in the separation computations by comparing one-dimensional and two-dimensional separations during a westward traveling surge passage over the network. The analysis yielded results similar to earlier ones [Küppers *et al.*, 1979; Richmond and Baumjohann, 1984] which

suggest that the one-dimensional separation gives quite reliable results under most of the situations considered.

## 5. Conclusions

1. At substorm onset,  $\sim 40\%$  of the disturbance measured by the  $AL$  index comes from subsurface currents and hence do not represent ionospheric currents. The internal contribution is largest for rapid time variations and decreases during the expansion and recovery phases to an average of  $\sim 15 - 20\%$  during nondisturbed times. This is significant when the maximum  $AL$  values are used for characterization of the energy dissipation in the ionosphere.

2. Because the inductive component rises rapidly during the onset time, the gradient in the  $AL$  index suggests more rapid growth of the ionospheric current system than in reality is the case. While the  $AL$  index typically would suggest values around 30 nT/min, the real change in the external current system is only  $\sim 15$  nT/min. This is important to include in studies of the substorm-associated ionospheric current systems.

3. The internal contribution is largest for highly conducting Earth such as seawater. Hence, stations surrounded by oceans measure  $\sim 10 - 20\%$  larger variations than inland stations. This should be noted when measurements from several stations are compared with each other. Furthermore, the details of the geometry of the current system affect the size of the inductive component.

4. Results presented here suggest a general rule-of-thumb where the maximum  $AL$  is reduced by 40% to get the external current contribution, the average correction during nononset times is  $\sim 15 - 20\%$  decrease of the measured variation for inland stations and 25-30% for stations close to oceans. For more detailed results, the separation should be performed for each case individually using a chain of magnetometers.

## Appendix A: Practical Procedure of the Field Separation

### A.1. Calculation of the separation integral

As shown in Section 2.1, inverse Fourier transform yields the separation integrals

$$\begin{aligned} X_{\text{ext}} &= \frac{1}{2}(X + KZ) \\ X_{\text{int}} &= \frac{1}{2}(X - KZ) \\ Z_{\text{ext}} &= \frac{1}{2}(Z - KX) \\ Z_{\text{int}} &= \frac{1}{2}(Z + KX), \end{aligned} \tag{A1}$$

where  $K$  is an operator defined by

$$Kf(x) = \frac{1}{\pi} \int_{-\infty}^{\infty} du \frac{f(u)}{x-u} \tag{A2}$$

The integral in (A2) has a singularity at the observation point  $x$ . However, following *Schmucker* [1970], we assume that the function  $f$  varies linearly between observation points. Then the singularity turns to a form of  $0 \cdot \ln(0)$ , which yields zero. The final result for  $Kf(x_n)$  computed at discrete points  $x_n (n = 1, \dots, N)$  is

$$Kf(x_n) \approx -\frac{f_N - f_1}{\pi} - \frac{1}{\pi} \sum_{m=1}^{N-1} (\bar{f}_m + (x_n - \bar{x}_m) f'_m) \ln \left| \frac{x_{m+1} - x_n}{x_m - x_n} \right| + \frac{f_n}{\pi} \ln \left| \frac{x_{n-1} - x_n}{x_{n+1} - x_n} \right|, \quad (\text{A3})$$

where in the summation  $m \neq n - 1, n$ , and the following notations are used:

$$\begin{aligned} \bar{x}_m &= \frac{x_m + x_{m+1}}{2} \\ \bar{f}_m &= f(\bar{x}_m) \approx \frac{f(x_m) + f(x_{m+1})}{2} \\ f'_m &= \frac{f_{m+1} - f_m}{x_{m+1} - x_m}. \end{aligned} \quad (\text{A4})$$

It is also possible to perform the separation by the Fourier transform. We made some tests with model data and found the difference between these methods to be only about 0-3 percent units. The Fourier transform seems to be slightly more accurate, but it requires interpolation of the original field into a regularly spaced  $x$  axis, whereas the spatial integration can be directly performed at the original observation points. The Fourier approach also has a similar systematic error as the spatial integration: the external to total field ratio tends to be slightly too small at the *AL* station.

## A.2. Consideration of One Dimensionality

The separation method used here requires that the horizontal field does not have a component perpendicular to the  $x$  axis. As such situations seldom happen in reality, this requires some specific tricks. One possibility is to rotate the  $x$  axis at each time step to a direction in which the transverse component is small at least in regions where the horizontal field is large [*Viljanen et al.*, 1995].

Another approach, applied here, is to keep the  $x$  axis fixed. Let us denote the ratio of the external component to the total  $X$  by  $\tilde{R} = X_{\text{ext}}/X_{\text{tot}}$ , which is calculated in the nonrotated  $xy$  frame. This is the correct result if the ionospheric current flows exactly in the  $y$  direction. If the direction of the ionospheric current deviates from the  $y$  axis by an angle  $\alpha$ , then

$$X_{\text{tot}}(x) = X'_{\text{tot}}(x') \cos \alpha \quad (\text{A5})$$

$$X_{\text{ext}}(x) = X'_{\text{ext}}(x') \cos \alpha,$$

where primed quantities refer to the  $x'y'$  frame in which the current flows parallel to the  $y'$  axis.

When we compute the integral (A1) in the  $xy$  frame, we get a value  $\tilde{X}_{\text{ext}}$  which is by definition

$$\tilde{X}_{\text{ext}}(x) = \frac{1}{2}(X_{\text{tot}}(x) + KZ(x)). \quad (\text{A6})$$

Substituting (A5) into (A6) we obtain

$$\tilde{X}_{\text{ext}}(x) = \frac{1}{2}(X'_{\text{tot}}(x') \cos \alpha + KZ(x)) \quad (\text{A7})$$

Because  $KZ(x)$  is the same in both coordinate frames, Eq. A1 gives

$$X'_{\text{ext}}(x') = \frac{1}{2}(X'_{\text{tot}}(x') + KZ(x)) \quad (\text{A8})$$

from which we can solve  $KZ(x)$ . Using (A5) we finally get for the correct ratio of  $X_{\text{ext}}/X_{\text{tot}}$  in the  $xy$  frame:

$$R(x) = \tilde{R}(x) \cos \alpha + \frac{1 - \cos \alpha}{2}. \quad (\text{A9})$$

Because typically  $\tilde{R} > 0.5$ , then  $R < \tilde{R}$ . This means that the ratio calculated in the nonrotated frame is systematically larger than the correct one. However, the difference is only 0-3% units for  $\alpha$  smaller than  $30^\circ$ .

**Acknowledgments.** We wish to thank all institutes maintaining the IMAGE magnetometer network. The work of E.T. and A.P. was supported by the Academy of Finland.

Michael Blanc thanks Wolfgang Baumjohann for his assistance in evaluating this paper.

## References

- Allen, J. H. and H. W., Kroehl, Spatial and temporal distributions of magnetic effects of auroral electrojets as derived from AE indices, *J. Geophys. Res.*, *80*, 3667, 1975.
- Amm, O., Direct determination of the local ionospheric Hall conductance distribution from two-dimensional electric and magnetic field data: Application of the method using models of typical ionospheric electrodynamic situations, *J. Geophys. Res.*, *100*, 21,473, 1995.
- Baker, D. N., A. J. Klimas, R. L. McPherron, and J. Büchner, The evolution from weak to strong geomagnetic activity: An interpretation in terms of deterministic chaos, *Geophys. Res. Lett.*, *17*, 41, 1990.
- Baker, D. N., T. I. Pulkkinen, V. Angelopoulos, W. Baumjohann, and R. L. McPherron, The neutral line model of substorms: Past results and present view, *J. Geophys. Res.*, *101*, 975, 1996.
- Bargatze, L. F., D. N. Baker, R. L. McPherron, and E. W. Hones Jr., Magnetospheric impulse response for many levels of geomagnetic activity, *J. Geophys. Res.*, *90*, 6387, 1985.
- Baumjohann, W., R. J. Pellinen, H. J. Opgenoorth, and E. Nielsen, Joint two-dimensional observations of ground magnetic and ionospheric electric fields associated with auroral zone currents: Current systems associated with local auroral break-ups, *Planet. Space Sci.*, *29*, 431, 1981.
- Birn, J., and M. Hesse, The substorm current wedge and field-aligned currents in the simulations of magnetotail reconnection, *J. Geophys. Res.*, *96*, 1611, 1991.
- Davis, T. N., and M. Sugiura, Auroral electrojet activity index AE and its universal time variations, *J. Geophys. Res.*, *71*, 785, 1966.
- Donovan, E. F., Modeling the magnetic effects of field-aligned currents, *J. Geophys. Res.*, *98*, 13,529, 1993.
- Häkkinen, L., and R. Pirjola, Calculation of electric and magnetic fields due to an electrojet current system above a layered Earth, *Geophysica*, *22*, 1-2, 31-44, 1986.
- Heinson, G., and S. Constable, The electrical conductivity of the oceanic upper mantle, *Geophys. J. Int.*, *110*, 159, 1992.
- Hermance, J. F., and W. R. Peltier, Magnetotelluric Fields of a Line Current, *J. Geophys. Res.*, *75*, 3351, 1970.
- Ieda, A., S. Machida, T. Mukai, Y. Saito, T. Yamamoto, A. Nishida, T. Terasawa, and S. Kokubun, Statistical analysis of the plasmoid evolution with Geotail observations, *J. Geophys. Res.*, *103*, 4453, 1998.

- Kallio, E. I., T. I. Pulkkinen, H. E. J. Koskinen, A. T. Viljanen, J. A. Slavin, and K. Ogilvie, Loading-unloading processes in the nightside ionosphere *Geophys. Res. Lett.*, *27*, 1627, 2000.
- Kamide, Y., A. D. Richmond, and S. Matsushita, Estimation of ionospheric electric field, ionospheric currents, and field-aligned currents from ground magnetic records, *J. Geophys. Res.*, *86*, 801, 1981.
- Kauristie, K., T. I. Pulkkinen, R. J. Pellinen, and H. J. Opgenoorth, What can we tell about the AE-index from a single meridional magnetometer chain?, *Ann. Geophys.*, *14*, 1177, 1996.
- Küppers, F., J. Untiedt, W. Baumjohann, K. Lange, and A.G. Jones, A twodimensional magnetometer array for groundbased observations of auroral zone electric currents during the International Magnetospheric Study (IMS), *J. Geophys. Res.*, *46*, 429, 1979.
- Lu, G., et al., Global energy deposition during the January 1997 magnetic cloud event, *J. Geophys. Res.*, *103*, 11,685, 1998.
- Mareschal, M., Modelling of natural sources of magnetospheric origin in the interpretation of regional induction studies: A review, *Surv. Geophys.*, *8*, 261, 1986.
- Maurer, H., and B. Theile, Parameters of the auroral electrojet from magnetic variations along a meridian, *J. Geophys. Res.*, *44*, 415, 1978.
- Mersmann, U., W. Baumjohann, F. Küppers and K. Lange, Analysis of an eastward electrojet by means of upward continuation of groundbased magnetometer data, *J. Geophys. Res.*, *45*, 281, 1979.
- Opgenoorth, H. J., R. J. Pellinen, H. Maurer, F. Küppers, W. J. Heikkila, K. U. Kaila, and P. Tanskanen, Ground-based observations of an onset of localized field-aligned currents during auroral break-up around magnetic midnight, *J. Geophys. Res.*, *48*, 101, 1980.
- Opgenoorth, H. J., R. J. Pellinen, W. Baumjohann, E. Nielsen, G. T. Marklund, and L. Eliasson, Three-dimensional current flow and particle precipitation in a westward travelling surge (observed during the Barium-GEOS rocket experiment), *J. Geophys. Res.*, *88*, 3138, 1983.
- Pirjola, R., On magnetotelluric source effects caused by an auroral electrojet system, *Radio Sci.*, *27*, 463, 1992.
- Pirjola, R., and A. Viljanen, Complex image method for calculating electric and magnetic fields produced by an auroral electrojet of finite length, *Ann. Geophys.*, *16*, 1434, 1998.
- Richmond, A.D., and W. Baumjohann, Three-dimensional analysis of magnetometer array data, *J. Geophys. Res.*, *54*, 138, 1984.
- Rostoker, G., J. C. Samson, F. Creutzberg, T. J. Hughes, D. R. McDiarmid, A. G. McNamara, A. Vallance Jones, D. D. Wallis, and L. L. Cogger, CANOPUS: A ground-based instrument array for remote sensing the high latitude ionosphere during the ISTP/GGS program, *Space Sci Rev.*, *71*, 743, 1995.
- Schmucker, U., Anomalies of geomagnetic variations in the southwestern United States, *Bull. Scripps Inst. Oceanogr.*, *13*, 1, 1970.
- Syrjäsoo, M., et al., Observations of substorm electrodynamic using the MIRACLE network, in *Substorms-4*, edited by S. Kokubun and Y. Kamide, pp. 111, Terra Sci., Tokyo, 1998.
- Vassiliadis, D., A. Klimax, D. N. Baker, and D. A. Roberts, A description of solar wind - magnetosphere coupling based on nonlinear filters, *J. Geophys. Res.*, *100*, 3495, 1995.
- Viljanen, A., K. Kauristie, and K. Pajunpää, On induction effects at EISCAT and IMAGE magnetometer stations, *Geophys. J. Int.*, *121*, 893, 1995.
- Viljanen, A., R. Pirjola and O. Amm, Magnetotelluric source effect due to 3D ionospheric current systems using the complex image method for 1D conductivity structures, *Earth Planets Space*, *51*, 933, 1999a.
- Viljanen, A., O. Amm, and R. Pirjola, Modeling geomagnetically induced currents during different ionospheric situations, *J. Geophys. Res.*, *104*, 28,059, 1999b.
- Weaver, J. T., On the separation of local geomagnetic fields into external and internal parts, *Z. Geophys.*, *30*, 29, 1964.

---

O. Amm, L. Häkkinen, R. Pirjola, A. Pulkkinen, T. I. Pulkkinen, E. I. Tanskanen, and A. Viljanen, Geophysical Research Division, Finnish Meteorological Institute, P.O. Box 503, FIN-00101 Helsinki, Finland. (eija.kallio@fmi.fi)

(Received May 10, 2000; revised September 13, 2000; accepted September 13, 2000.)